DOI: 10.1002/cphc.200600029

CO Combustion on Supported Gold Clusters

Matthias Arenz,[a] Uzi Landman,[b] and Ueli Heiz*[a]

Recent progress in the understanding of the fascinating catalysis of CO combustion by supported gold particles is summarized. Focusing on size-selected gold clusters consisting of only a few atoms, that is, the size regime with properties nonscalable from the bulk properties, we discuss the current knowledge of the different factors controlling the reactivity at the molecular level. These factors include the role of the oxide support, its defects, cluster charging as well as the structural fluxionality of clusters, the cluster size dependency, and the promotional effect of water. By combining experimental results with quantum mechanical ab initio calculations, a detailed picture of the reaction mechanism emerges. While similar mechanisms might be active for gold nanoparticles in the scalable size regime, it is shown that for different systems (defined by the cluster size, the support, experimental conditions, etc.) the reaction mechanism differs and, hence, no generalized explanation for the catalytic driving force of small gold particles can be given.

Introduction

There are several reasons why gold has for a long time been regarded as a poor catalyst in heterogeneous catalysis. Most importantly, gold is the most noble of all metals in the bulk form. This property is due to the qualities of low adsorption energy of gases and high dissociation barriers, which are important for most catalytic reactions.[1] Furthermore, the low melting point of gold hampers the preparation of nanoparticles smaller than 10 nm in diameter,[2] which is crucial for maximizing the active surface area of a catalyst. First results which indicated that small gold particles might nevertheless be interesting for catalyzing reactions were reported in the early 1970s.[3,4] However, it was the work of Haruta et al.[2,5,6] which clearly established the exciting catalytic properties of gold nanoparticles. In 1983 they developed a method for preparing hemispherical gold particles on selected metal oxides, and showed that gold nanoparticles exhibit high catalytic activity for reactions such as CO oxidation and propylene epoxidation, especially at low temperatures.[5] CO oxidation was reported at temperatures as low as 200 K, which makes gold interesting for a series of applications at room temperature. Since then a huge number of papers have been published aimed at trying to understand the special catalytic properties of gold nanoparticles, that is, particles 1–5 nm in diameter. Possible applications are manifold; for example, the hydrochlorination of acetylene using carbon-supported gold catalysts has been investigated by Hutchings et al.[7,8] For further examples, see refs. [2, 6, 9–11] and references therein.

In the following a short overview of the combustion of CO on gold nanoparticles will be given. In early papers a classical Langmuir–Hinshelwood mechanism was assumed for the reaction involving the dissociation of oxygen molecules on Au,[12] as is the case for platinum-group metals. The catalytic activity of gold nanoparticles was thus explained by an increased heat of adsorption of oxygen atoms, produced by a hot filament on gold nanoparticles, compared to that of bulk gold.[12,13] Newer results, however, indicated that the way in which gold acts catalytically is substantially different from that of other noble metals.[11] For example, it is now well-established that independent of the substrate, molecular O_2, most likely O_2^-, reacts with CO to form CO_2 and no oxygen dissociation occurs upon adsorption on gold nanoparticles.[14–16] Henry et al. showed that, on reactive Au particles after adsorbing oxygen and pumping of the oxygen in the chamber, no adsorbed oxygen can be titrated by CO pulses any more, thus excluding the dissociative adsorption of oxygen.[17] In fact, it seems that the relatively weak adsorption energy of oxygen on gold and the formation of "activated" oxygen molecules are the key for low-temperature catalysis.

Despite the number of publications concerning CO oxidation on gold nanoparticles, the reaction mechanism and the factors controlling the reactivity are still not well understood. This is partially due to the variety of supports and preparation procedures used, which leads to contradictory reports on the catalytic activity and the importance of the experimental variables. In their review, Bond and Thompson[11] summarized as *consensual* observations the facts that i) oxide-supported small gold particles show the highest reactivity at sizes of about 2 to 3 nm, whereas unsupported gold particles are weakly active at best; and ii) the choice of support, the method of preparation, and the pretreatment before use are very important factors that control the reactivity. They discussed a possible mechanism involving reaction at the edge of a particle that included the support, thus emphasizing the importance of the perimeter interface. Similarly, Haruta recently reported[2] that the per-

[a] *Dr. M. Arenz, Prof. Dr. U. Heiz*
Lehrstuhl für Physikalische Chemie I, Technische Universität München
Lichtenbergstrasse 4, 85747 Garching (Germany)
Fax:(+49) 89-28913389
E-mail: ulrich.heiz@mytum.de

[b] *Prof. Dr. U. Landman*
School of Physics, Georgia Institute of Technology
Atlanta, GA 30332-0430 (USA)

formance of Au nanoparticles is defined by three major factors: the contact structure to the oxide support, the nature of the support, and the particle size, with the contact structure being the most important. The proposed perimeter model implies the direct involvement of the support in the CO oxidation reaction.[18] Furthermore, an enhancement of the catalytic activity of small gold particles due to moisture was reported.[19,20] This is particularly interesting for applications under ambient conditions, since the presence of moisture is commonly found to be detrimental to the activity of the particles. In contrast to the perimeter model of Haruta, Goodman and Choudhary[21] concluded, on the basis of a bilayered Au model catalyst which blocks the access of the support by the reactants, that the TiO_x support acts mainly as a dispersant and a promoter. Theoretical studies also highlight the importance of the periphery of the interface between a gold particle and the oxide support. Furthermore, it has been suggested that the propensity of O_2 to adsorb on finite-size Au particles is increased, particularly at low-coordinated sites.[16,22–26] The importance of low-coordinated sites is in line with the experimental work on supported gold model catalysts by Freund et al.[27–29] They emphasize the influence of highly uncoordinated gold atoms on the CO adsorption properties. To summarize, the variety of different preparation procedures, pretreatment conditions, and supports, the often undefined catalysts, and the strong interdependence of these factors with the observed catalytic activity prevent a uniform description of the processes involved.

To disentangle the factors controlling the reactivity of gold, it is thus helpful to study the underlying concepts on well-defined model systems. In this Minireview, we summarize the work covering CO combustion on *size-selected* gold particles supported on thin oxide films. The size of the particles is below 1 nm in diameter, that is, the size regime in which the electronic, and thus catalytic, properties of the particles are not scalable from the bulk properties. In contrast to the work on gold nanoparticles, the systems discussed are exclusively model catalysts on planar supports. The focus is on work from our laboratory in combination with extensive ab initio calculations.

The Size-Dependent Reactivity of Supported Au_n Clusters

Au_n clusters were produced by a laser vaporization source,[30,31] size-selected in a quadrupole mass spectrometer, and deposited with low kinetic energy (<0.2 eV/atom, that is, soft landing) on thin oxide films.[32,33] One concern when using free clusters to prepare monodispersed cluster materials is the fate of the deposited cluster during and after deposition. In addition to molecular dynamics simulations,[34] several experiments, such as STM investigations[35,36] or absorption spectroscopy of clusters embedded in a rare-gas matrix, have been performed, which demonstrate that soft landing of clusters is possible.[37] Also, the studies of the chemical reactivity of supported clusters using pulsed molecular beams show evidence of stability of the samples.[38] Recently, we were able to prove the monodispersion of the cluster with cavity ringdown spectroscopy.[39]

Supported, small gold clusters have mainly been deposited on thin MgO(100) films. These thin films can be prepared either as defect-rich films, characterized by a given density [$\approx 5\%$ monolayer (ML) of extended defects and point defects [F centers (FC)], or as defect-poor films with a negligible density of F centers.[14,40] In our laboratory the CO oxidation reaction was studied by a combination of temperature-programmed reaction (TPR) and Fourier-transform infrared (FTIR) spectroscopy. Isotopically labeled $^{18}O_2$ and ^{13}CO molecules were used in these experiments, and the catalytic oxidation of CO involving oxygen atoms from the MgO substrate is excluded, since only the $^{13}C^{16}O^{18}O$ isotopomer was detected. Bare MgO films, defect-poor as well as defect-rich, are inert to CO oxidation.[14]

As demonstrated in Figure 1, gold clusters up to the heptamer are inert to CO oxidation on defect-rich MgO and the smallest size for which the low-temperature ($T<250$ K) combustion was detected is Au_8. For larger sizes a distinct size dependency is observed (Figure 1 a), with roughly two temperature regions for CO oxidation, $T<250$ and >250 K, which are associated with different reaction mechanisms (see below). As expected, gold films are inert to CO oxidation. By integrating the total area in the mass spectra, the total number of CO_2 molecules formed per cluster can be plotted versus the number of atoms per cluster (Figure 1 b). No linear dependency of the reactivity as a function of size is observed, which clearly indicates that the number of reactive sites differs for each cluster size. Recently, Anderson et al.[41,42] started to investigate the CO oxidation reaction on size-selected gold clusters; they used a TiO_2(110) single crystal as substrate. By employing

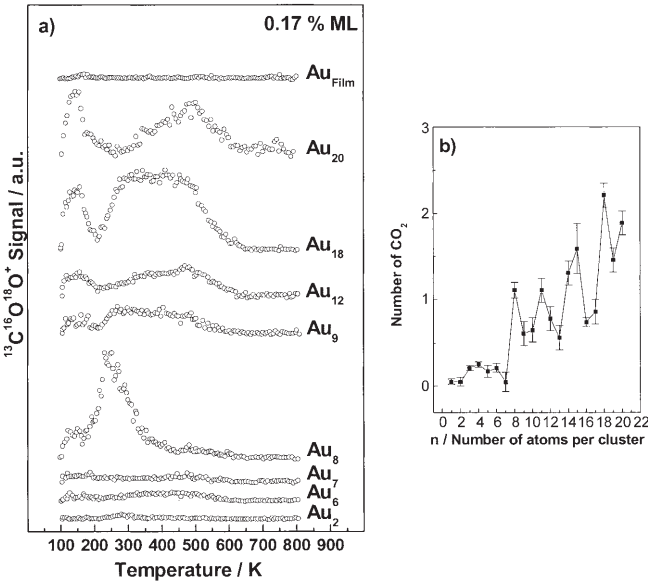

Figure 1. a) Temperature programmed reaction experiments for the CO-oxidation on selected Au_n clusters on defect-rich MgO(100) films. The model catalysts are saturated at 90 K with ^{13}CO and $^{18}O_2$ and the isotopomer $^{13}C^{18}O^{16}O$ is detected with a mass spectrometer, as a function of temperature; b) The reactivities for Au_n expressed as the number of formed CO_2 per cluster.

pulsed molecular CO beams at room temperature, small activities for cluster sizes even smaller than Au_8, that is, Au_n with $n=3$–7, were reported. For Au_7, a steep increase in reactivity is observed. Notably, the cluster density for Au_7 is ten times lower than on all other surfaces and, hence, the steep increase in CO_2 molecules formed per Au atom (by a factor of about 10) might be due to calibration problems. Nevertheless, these results demonstrate a strong dependence of the substrate on the reactivity of Au clusters.

The Reaction Mechanism

Turning our attention to the reaction mechanism for CO oxidation on gold clusters supported on MgO films, two characteristics are important. As exemplified in the TPR spectra of Au_8 supported on defect-poor and defect-rich MgO films (Figure 2),

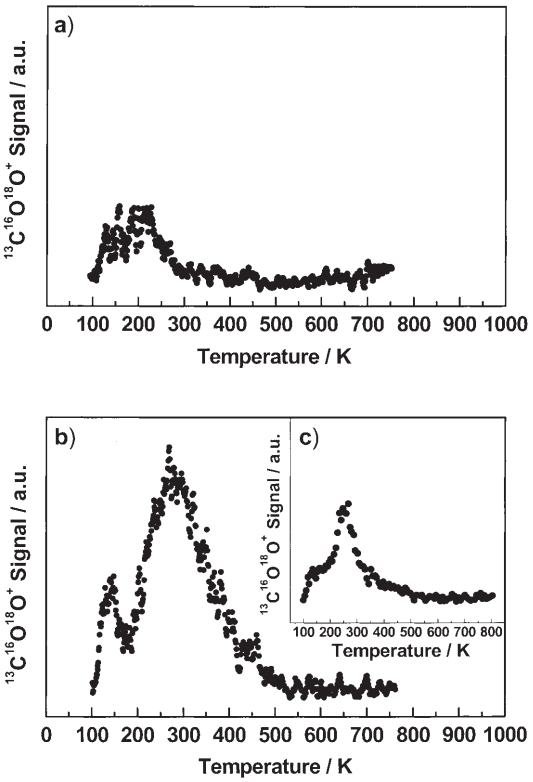

Figure 2. Temperature programmed reaction experiments for the CO-oxidation on Au_8 clusters on a) defect-poor and b) defect-rich MgO(100) films; inset c) shows the results after producing FC on MgO(100) after the procedure of Pfnür et al. The model catalysts are saturated at 90 K with ^{13}CO and $^{18}O_2$ and the isotopomer $^{13}C^{18}O^{16}O$ is detected with a mass spectrometer, as function of temperature.

the reactivity is strongly dependent on the number of defects on the support (see below); second, for reactive gold clusters (see also Figure 1), two temperature regions are observed at roughly $T<250$ and >250 K. In the two temperature regions, two different reaction pathways may contribute to the oxidation of CO. Notice that due to the reaction conditions,[14] peaks in the TPR spectra can be associated with Langmuir–Hinshelwood (LH) types of reaction mechanisms. Extensive ab initio calculations of the reaction mechanism on Au_8/MgO indicate two different LH-type mechanisms. Correlated to the formation of CO_2 at 140 K (Figure 3 a–c), the two reactants are initially co-

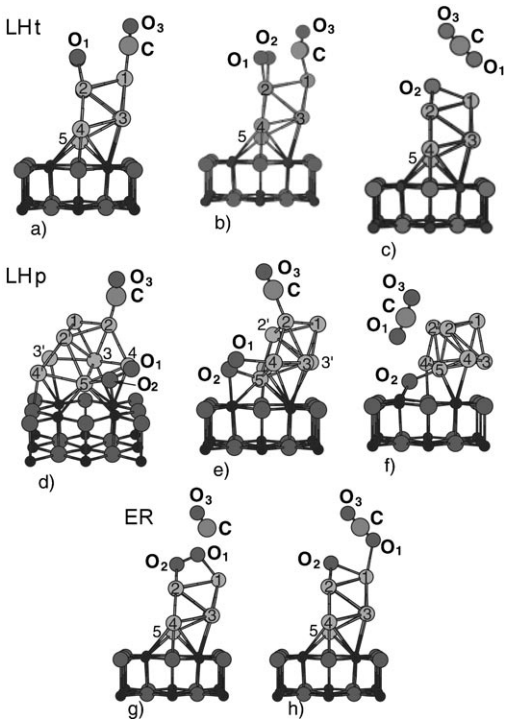

Figure 3. Reaction mechanisms of the CO oxidation on Au_8.

adsorbed on the triangular top facet of the Au_8, therefore termed the LHt mechanism. The distance between the carbon atom and one of the peroxo oxygen atoms in this local minimum state is equal to 3.11 Å [$d(CO_1)$]. Through mapping of the potential energy surface along the C–O_1 reaction coordinate, a rather low energy barrier ΔE_b (LHt) = 0.1 eV occurring at $d(CO_1) \approx 2.0$ Å is determined for the LHt oxidation channel, with the end product a weakly adsorbed carbon dioxide molecule (≈0.2 eV). This LHt low-temperature oxidation mechanism occurs, in these theoretical studies (with similar energetics), for reactions on the gold cluster deposited on either a defect-free MgO(100) surface, or on one containing an F_{5c} defect site.[14] Both are expected to be relatively insensitive to the Au_n cluster size, thus correlating with the experimental results (Figures 1 and 2).

As shown in Figure 2, the higher-temperature channel is strongly enhanced for Au_8 supported on a defect-rich (compared to a defect-poor) MgO(100) support. This trend correlates with the simulations of an LH periphery (LHp) reaction mechanism, which starts with a CO molecule adsorbed on the top facet of the Au_8 cluster and a peroxo O_2* molecule bonded to the periphery of the interfacial layer of the cluster (where the distance between the C atom and the oxygen atom marked O_1 is $d(CO_1) = 4.49$ Å). Indeed, mapping of the potential energy surface along the C–O_1 reaction coordinate reveals for

$Au_8/MgO(F_{5c})$ a rather broad reaction barrier $\Delta E_b(LHp) \approx 0.5$ eV at $d(CO_1) \approx 2.0$ Å (Figure 3), while for the defect-free substrate a significantly higher barrier of $\Delta E_b(LHp) \approx 0.8$ eV is found; the reaction product is shown in Figure 3 f for the $Au_8/MgO(F_{5c})$ catalyst. This change in activation energy is at the origin of the observed change in reactivity, as for the defect-poor substrate the CO molecule desorbs prior to reaction. The question may arise as to why the two reaction channels are observed experimentally, as the low-temperature mechanism should always be dominant because its reaction rate is orders of magnitude higher. In fact, theoretical studies reveal that only one oxygen molecule adsorbs on the clusters. Thus, there exists an ensemble of Au_8 with an oxygen molecule adsorbed on the periphery, and another ensemble with the oxygen molecule bound to the top facet of the cluster. In fact, the ratio of the number of CO_2 molecules formed at low and high temperature is in the same range as the ratio of O_2 molecules that directly adsorb on Au_8 (leading to O_2 adsorbed on the top facet of Au_8), and which adsorb via reverse spillover from the MgO substrate (leading to O_2 adsorbed on the periphery of Au_8).

In addition to the two LH-type mechanisms, a third reaction path was found in the calculations, which starts from the optimal configuration of O_2* adsorbed on the $Au_8/MgO(F_{5c})$ catalyst. A gas-phase CO molecule brought into the vicinity of the peroxo molecule reacts spontaneously (without an energy barrier), to form a CO_2 molecule weakly bound to the catalyst. Therefore, this reaction (Figure 3 g,h) corresponds to an Eley–Rideal (ER)-type mechanism, which can occur even at 90 K, that is, during the initial dosing stage in the experiment.

The Role of the MgO Substrate

In the following discussion, we take a closer look at the influence of surface defects on the activity of the smallest active gold cluster on MgO, that is, Au_8. As discussed above, the strong influence of defect structures of the MgO substrate on the reactivity of Au_8 is apparent in the experiments (Figure 2). An important class of point defects in MgO is oxygen vacancies; their direct characterization on the surface, however, is not straightforward. Only recently, singly charged surface oxygen vacancies (F^+ centers) have been characterized by electron paramagnetic resonance (EPR) measurements by Freund et al.[43] Neutral F centers are not susceptible to EPR spectroscopy, but have been investigated by scanning tunneling microscopy and spectroscopy (STM and STS, respectively).[44,45] On MgO films prepared with low deposition rates, Au_8 is almost inert; however, Au_8 becomes active on defective MgO(100) films prepared with high deposition rates.[14] On the latter films Au_8 forms CO_2 at 140 and 280 K. Note that these observations are independent of the preparation procedure for defect-rich MgO films; that is, films prepared by high deposition rates show the same results as films with a high density of F centers prepared after the methodology of Pfnür et al.[46] (see Figure 2 c). This finding suggests that F centers play a crucial role in the reactivity of Au_8.

The influence of F centers on MgO(100) films on the reactivity of gold clusters is studied in more detail by FTIR spectroscopy, using CO as both reactant and probe molecule. These experiments are combined with extensive DFT calculations. In the FTIR spectra shown in Figure 4, CO stretching frequencies at 2102 and 2077/2049 cm^{-1} (Au_8 on defect-poor and defect-rich films, respectively) are observed as well as a band at 1300 cm^{-1}, which is tentatively attributed to highly activated

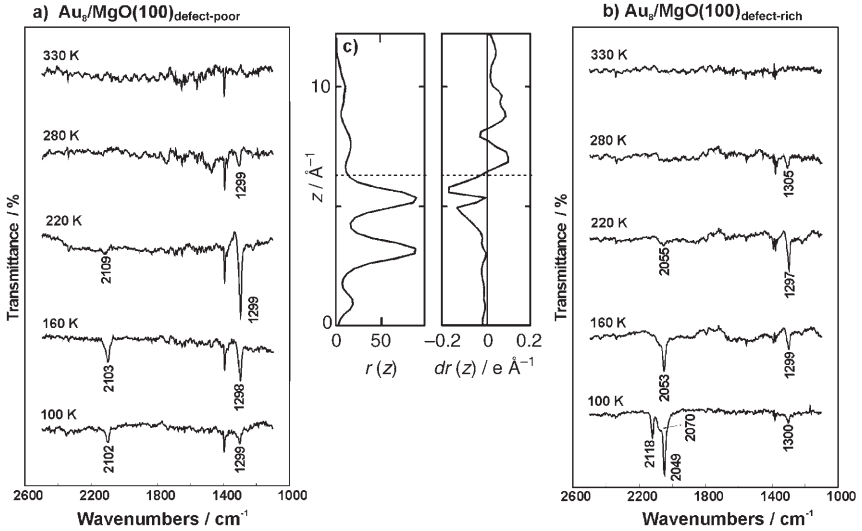

Figure 4. FTIR spectra taken at 90 K after exposing the model catalysts a) $Au_8/MgO(100)_{defect\text{-}poor}$ and b) $Au_8/MgO(100)_{defect\text{-}rich}$ to ^{13}CO and O_2 and annealing the sample at the indicated temperature. The frequencies between 2050–2100 cm^{-1} are attributed to adsorbed CO, whereas the band at 1300 cm^{-1} may originate from activated O_2 molecules. Note, the redshift of the CO-stretch by 50 cm^{-1} on defect-rich films. This shift is consistent with the predicted charging of the cluster when deposited on an F center (c), where the difference of the charge densities of the isolated (Au_8, MgO_{5Fc}) and the model system (Au_8/MgO_{5Fc}) is calculated. The charging is estimated to be 0.5 e^-.

O_2, thus indicating that both reactants (CO and O_2) are adsorbed molecularly at 90 K.[15] For the reactive model catalyst these vibrational bands disappear in concert with the formation of CO_2 (Figure 4 a) whereas, in the case of the unreactive model catalyst [Au_8/MgO(defect-poor)], the two reactants simply desorb from the sample, as monitored by mass spectrometry.[14,15] From theoretical studies, three energy-optimized deposited cluster configurations pertinent to the experimental conditions are obtained (Figure 5). The bare adsorbed Au_8 cluster (Figure 5 a) exhibits only a slight distortion from the structure of the corresponding gas-phase neutral cluster.[15] However, the strong influence of F centers is reflected in the calculated binding energy of Au_8 to the defective MgO surface (3.445 eV) and to the defect-free surface (1.225 eV). For details

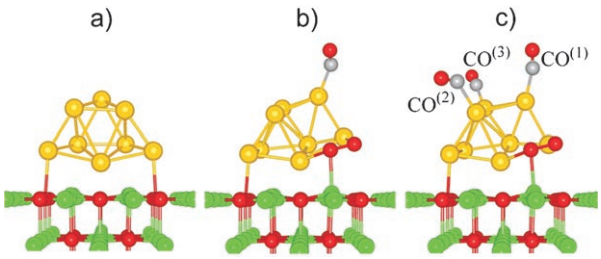

Figure 5. Optimized configurations of a) a bare gold octamer (yellow spheres), adsorbed on an F-center of an MgO (001) surface (oxygen atoms in red and magnesium in green); b) a surface-supported gold octamer with an oxygen molecule, adsorbed at the interface between the cluster and the magnesia surface. Note, the significant change in the geometry of the cluster compared to the one shown in (a); c) the gold octamer on the magnesia surface (MgO(FC)) with three CO molecules (carbon in grey and oxygen in red), adsorbed on the top facet of the cluster and an oxygen molecule, pre-adsorbed at the interface between the cluster and the magnesia surface. Note, that the molecule marked $CO^{(2)}$ lies parallel to the surface and is thus, not infra-red active in the experimental configuration employed here. The C–O bond length $d(CO^{(i)})$, the charge transferred to the $CO^{(i)}$ molecule $\Delta Q^{(i)}$, and the calculated C–O vibrational frequency $\nu^{(i)}$, $i=1,2$, and 3, as well as the corresponding values for the O_2 molecule, are: $d(CO^{(i)})$ [Å] = 1.151, 1.158, 1.153, $d(O_2)=1.422$; $\Delta Q^{(i)}$ [e] = 0.306, 0346, 0.319, $\Delta Q(O_2)=1.125$; $\nu^{(i)}$ [cm^{-1}] = 1993, 1896, 1979, $\nu(O_2)=895$.

decrease in frequency (61 cm^{-1}) in comparison to the value calculated for the free molecule is attributed to a net excess charge (0.285 e^-) on the adsorbed molecule, which results from back-donation into the CO($2\pi^*$) antibonding state. As expected, such donation of charge from occupied orbitals of the metal to unoccupied states of the adsorbed molecule is even more pronounced (0.878 e^-) for the more electronegative dioxygen molecule. Upon charging the complex with up to 0.5 e^-, the net excess charge on the ^{13}CO molecule is increased to 0.341 e^- and is reflected in a red shift of the CO stretching frequency (1975 cm^{-1}) by 34 cm^{-1} with respect to the neutral cluster case (2009 cm^{-1}). Concurrently, the C–O bond length is increased (see Table 1). A similar behavior is also found when starting from the triplet state of the neutral complex. The actual degree of charge transfer can be deduced directly from ab initio calculations, where the charge density of the Au_8/MgO(F_{5c}) system is compared with that of the isolated system [Au_8, MgO(F_{5c})].[14,15] The difference in the two charge-density plots predicts a charge transfer of 0.5 e^- into the cluster (see middle part of Figure 4). Comparing theory and experiment, the experimentally observed red shift in the C–O stretch for the molecule adsorbed on differently prepared MgO (defect-rich and defect-poor) films is thus direct experimental evidence of the DFT calculations, see ref. [15]. Optimal geometries with a single adsorbed CO molecule, Au_8/O_2/CO/MgO(FC), and at saturation coverage of the cluster [that is, with three adsorbed CO molecules, $Au_8/O_2/(CO)_3$/MgO(FC)] are shown in Figures 5a and b, respectively. From the three adsorbed ^{13}CO molecules at saturation coverage, only two have a significant dynamic dipole moment perpendicular to the surface, $CO^{(1)}$ and $CO^{(3)}$, consistent with the experimental observation (Figure 4).

Table 1. Vibrational frequencies of the $Au_8O_2{}^{13}CO$ complex (gas phase) as a function of charging.[a]

ΔQ ($Au_8O_2{}^{13}CO$)	Spin	ν [cm^{-1}]	BE ($O_2+{}^{13}CO$) [eV]	$d(^{13}CO)$ [Å]	ΔQ (^{13}CO)	$d(O_2)$ [Å]	ΔQ (O_2)
0	1	2005	1.060	1.149	0.29	1.336	0.71
0.25	0.875	1987		1.150	0.32	1.344	0.75
0.5	0.75	1968		1.154	0.35	1.350	0.77
1.0	0.5	1926		1.160	0.43	1.364	0.86
0	0	2009	0.753	1.148	0.28	1.378	0.88
0.25	0	1990		1.150	0.31	1.381	0.89
0.5	0	1975		1.153	0.34	1.385	0.92
1.0	0	1920		1.158	0.41	1.398	1.00

[a] Results for free ($Au_8O_2{}^{13}CO$) complexes as a function of excess electron charge ΔQ. The results are shown for various values of the spin; for the neutral cluster, triplet ($S=1$) and singlet ($S=0$) states. The displayed quantities are: ν, the CO stretch frequency; BE($O_2+{}^{13}CO$), the CO binding energy to the gold cluster with a pre-adsorbed oxygen molecule; the bond distances, $d(^{13}CO)$ and $d(O_2)$, and excess electronic charges, $\Delta Q(^{13}CO)$ and $\Delta Q(O_2)$, of the two adsorbed reactants CO and O_2. For reference, the calculated vibrational frequency of gas-phase ^{13}CO is 2070 cm^{-1}, which is 25 cm^{-1} smaller than the experimental value of $\nu(^{13}CO)=2095$ cm^{-1}.

The key for understanding the influence of F centers on the reactivity of Au_8 is the experimentally observed red shift in the CO stretching frequency, by 25–50 cm^{-1} for CO/Au_8/MgO(defect-rich) compared to CO/Au_8/MgO(defect-poor). This shift indicates a change in the charge state of the gold octamer bound to the defective magnesia surface, since the absorption frequency of CO adsorbed on metal surfaces depends strongly on the population of the antibonding $2\pi^*$ orbital. Table 1 summarizes the calculated influence of excess charge ΔQ for the isolated $Au_8/O_2/{}^{13}CO$ complex. The calculations clearly show that the ^{13}CO stretching frequency shifts as a function of the charge state of the complex. In detail, the shift is correlated with variations in the population of the antibonding state. For neutral complexes [ΔQ ($Au_8/O_2/{}^{13}CO$) = 0 in Table 1] with zero spin, a vibrational frequency of 2009 cm^{-1} is obtained for the adsorbed ^{13}CO. The calculated of the existence of a high concentration of F centers on our defect-rich MgO films.

The consequences of the charge transfer from the oxygen vacancy into the deposited Au_8 cluster for the binding and activation of the two reactants can be outlined by analyzing the local density of electronic states (LDOS) projected on the oxygen molecule, adsorbed at the periphery site of Au_8/MgO(F_{5c}) (Figure 6a). All the prominent peaks can be unambiguously assigned to orbitals of (free) molecular oxygen origin. In addition, these states overlap with the entire d band of the Au_8 cluster (Figure 6b) in the range of -7 eV $\leq E \leq E_F$, where E_F is the Fermi energy. Bonding of the oxygen molecule to the gold octamer involves mainly hybridization of the 5σ, $1\pi_{\parallel}$, and $1\pi_{\perp}$ oxygen states with the gold d band. Most importantly, the full

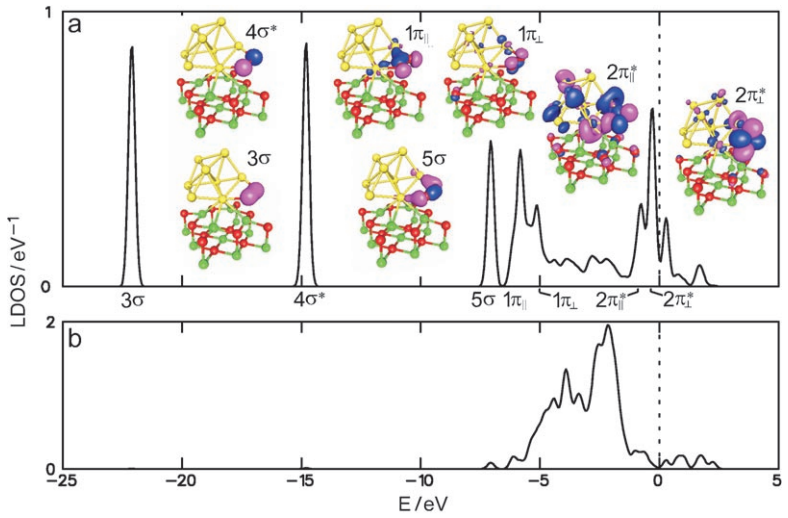

Figure 6. Local density of the electronic states (LDOS) of $Au_8/O_2/MgO(100)FC$. For these studies the O_2 molecule is adsorbed on the periphery and no CO molecules are co-adsorbed in order to separate the interaction of O_2 with the cluster from coupling effects between the reactants. The prominent peaks of the oxygen LDOS are labeled following the conventional nomenclature for the molecular orbitals of the gas-phase O_2 molecule, with $\perp$ and $\parallel$ meaning perpendicular and parallel to the MgO surface, respectively. The Fermi energy is a 0 eV.

relation diagram of the cluster complex bound to the defect-free MgO surface, where back-donation, however, is less pronounced.

Electronic Size Effects

Understanding the size-dependent electronic structure of the $Au_n/MgO(F_{5c})$ model catalysts is fundamental for elucidation of their atom-by-atom controlled reactivity. As discussed above, bonding and activation of O_2 at the periphery site of the $Au_8/MgO(F_{5c})$ model catalyst is enabled by resonances formed between the cluster's electronic states and the $2\pi^*$ molecular states of oxygen. A drastically

spin-manifold of the antibonding $2\pi^*$ states of O_2 is located below E_F, which results in strong activation of the O_2 molecule through occupation of the antibonding orbitals. This leads to weakening of the O–O bond, which is reflected in a significant increase of its length (1.43 Å) compared to that of the free molecule (1.25 Å), and the molecule is adsorbed in a peroxo-like state.[15] We observe that O_2 binding to the cluster is stronger in the presence of the F center (0.469 and 0.329 eV for the spin 0 and spin 1 states, respectively) in comparison to the case without F centers (0.329 and 0.299 eV for the spin 0 and spin 1 states, respectively). The bonding of CO to the $Au_8/O_2/MgO(FC)$ complex can be understood by analyzing the correlation diagram shown in Figure 7. It depicts the LDOS for the two reactants, CO (Figure 7a) and the $Au_8/O_2/MgO(FC)$ complex (Figure 7c), as well as for the product complex $Au_8/O_2/CO/MgO(FC)$ with the CO adsorbed on the deposited cluster (Figure 7b). As expected, the 3σ and the nonbonding 4σ molecular orbitals of the isolated CO are not involved in the bonding to the cluster complex as their energies are not changed upon adsorption. On the other hand, the nonbonding 5σ orbital is stabilized by the interaction (by about 3 eV), and thus it contributes to the chemisorption of carbon monoxide to the surface-supported complex through hybridization with the metal-cluster orbitals. The 1π level is slightly pushed upward in energy (<1 eV). The largest contribution to the bonding of CO to the complex occurs via hybridization of the antibonding $2\pi^*$ levels of CO and the occupied frontier electronic states of the cluster complex. The $2\pi^*$ orbitals are pushed below the Fermi level, partially populating this molecular state, namely, the so-called back-donation.[47] All these features are also present in the cor-

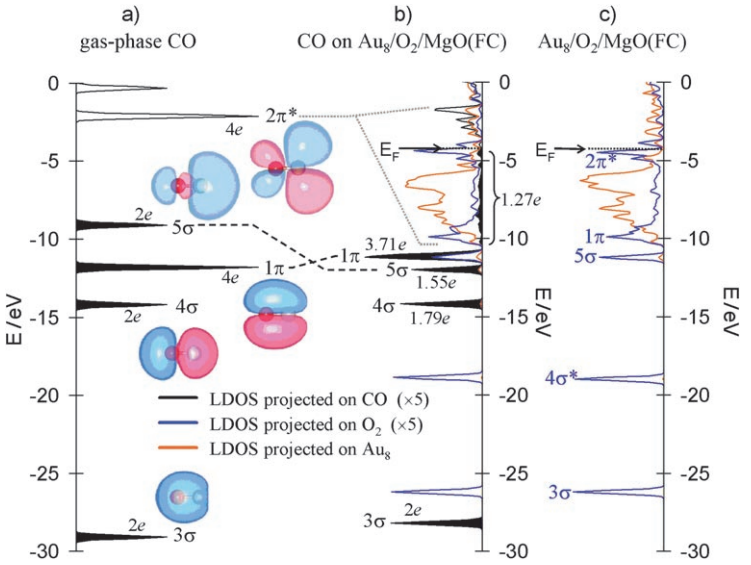

Figure 7. Local density of states (LDOS) correlation diagrams of a) free CO and b) complex $Au_8/O_2/CO/MgO(FC)$ and c) free $Au_8/O_2/MgO(FC)$. The electron populations of the various levels are given as 2*e*, 4*e*, etc., and iso-surface images of the orbitals of the free CO molecules are also shown (left). Dashed lines indicate orbital shifts and redistribution, caused by the adsorption of the CO molecule.

different scenario is found for the interaction of O_2 with a smaller gold cluster, $Au_4/MgO(F_{5c})$, where molecular oxygen adsorbs in an "on-top" configuration, with one of the oxygen atoms binding to a single gold atom (not shown).[48] This system exhibits rather weak binding of the molecule to the metal cluster (0.18 eV) and an almost unperturbed O–O bond length. The weak binding can be attributed to the narrower d band of the adsorbed Au_4 cluster compared to that of Au_8, with a consequent lack of overlap between the states at the bottom of the d band of the gold cluster and the molecular

oxygen states, with energies $E < -5$ eV. Moreover, the antibonding $2\pi^*_{\perp}$ and $2\pi^*_{\parallel}$ orbitals of the adsorbed oxygen molecule are located above E_F, which results in no activation of the molecule by the adsorbed Au_4 cluster. For further details, see ref. [48].

Structural Dynamical Fluxionality

The capability of small clusters to exhibit several structural forms (isomers) of comparable energies, and to interconvert between such isomers at finite temperature, is one of the hallmarks of cluster science. This unique structural variability may influence the chemical reactivity of nanocatalytic systems in two main ways. First, at finite temperature, the model catalyst will form an equilibrium ensemble of coexisting structural configurations, with various isomers exhibiting different chemical reactivities. Second, and most important, is the structural dynamic fluxionality of clusters, which in the course of reactions expresses itself in the ability of a given structural isomer to dynamically adapt its structure, such as to allow the reaction to evolve on the most favorable free-energy path. Such a fluxional propensity is illustrated in Figure 5a–c, which compares the bare-cluster geometry with those of the gold cluster with adsorbed reactant molecules, and is essential for the reaction to occur, since it was found that constraining the cluster to maintain its original geometry prevents the adsorption and activation of O_2.[14]

The Effect of Water

As mentioned in the Introduction, for certain supports, moisture is able to increase the activity of gold nanocatalysts by about two orders of magnitude.[20] Thus, the influence of water on the chemical activity of gold clusters was recently investigated by quantum mechanical ab initio calculations for Au_8 adsorbed on a defect-free MgO(100) surface,[49] that is, a system that does not exhibit charging effects and is inert to CO oxidation (see above). The calculations were based on spin-density functional theory, with generalized gradient corrections (CGA).[50] The wavefunctions are expanded in a plane-wave basis, with a kinetic energy cutoff of 25 Ry. The core–valence interactions for Au, O, and H are described through the use of ultrasoft pseudopotentials,[51] and a norm-conserving pseudopotential is used for Mg.[52] For further details of the calculations and the determination of the binding energies, the interested reader is referred to the original literature.[49]

The influence of water (co)adsorption manifests itself in the calculated change of the oxygen binding energies. For the gold octamer bound to a defect-free MgO(100) surface, two spatial regions for oxygen adsorption may be identified in calculations: i) the top facet of the cluster, where O_2 adsorbs weakly (adsorption energies up to 0.1 eV), in agreement with the results in refs. [14, 23, 26], and ii) peripheral sites (at the Au_8/MgO interface), where O_2 adsorbs with energies between 0.3 and 0.8 eV (Table 2), with the O–O bond extended to 1.37–1.49 Å. Water adsorbs (relative weakly) on free and supported Au clusters (Table 2), with adsorption energies that vary from 0.2 to 0.6 eV, and without apparent correlation between the adsorption strength and the coordination of the adsorption site. Interestingly, it was found that an adsorbed H_2O molecule is an "attractor" for molecular O_2, and in the presence of an adsorbed water molecule O_2 preferentially adsorbs at a neighboring site. Moreover, it may bind even at sites where the adsorption of O_2 (without coadsorbed H_2O) is energetically unfavorable.

Table 2. Energies [in eV] for the adsorption and coadsorption of O_2 and H_2O on free Au_8 and on a gold octamer supported on MgO(100), that is, Au_8/MgO. In the case of the Au_8/MgO system, results are given for both the adsorption on the top facet of the gold cluster (T) and at the peripheral interface of the cluster with the substrate (P).

	O_2	H_2O	H_2O–O_2
Au_8	unbound	$\approx$0.3	0.4–0.9
Au_8/MgO-T	$\leq$ 0.1	0.2–0.3	0.5–1.2
Au_8/MgO-P	0.3–0.8	0.4–0.6	1.3–2.1

In some cases when H_2O and O_2 coadsorb on the top facet of Au_8/MgO, the proton shared by the H_2O and O_2 molecules may actually be considered as transferred to the O_2 species and an OH and a hydroperoxyl-like (HO_2) group are formed (for details, see ref. [49]). The distance between the O atoms sharing the proton takes a value of $\approx$2.49 Å, while the O–O hydroperoxyl bond length reaches a value of about 1.48 Å (that is, 21% larger than in a free molecule), thus reflecting a very high degree of bond activation. A charge analysis shows that an amount of approximately 0.31 e^- is transferred from the Au_8/MgO system to the coadsorbed species. These results suggest that the coadsorption of H_2O and O_2 stabilizes the partially charged, highly activated states of the adsorbed oxygen molecule. No such bond activation is found for the adsorption of O_2 on the top facet of the supported gold octamer without water coadsorption. MgO surfaces are hydrophilic and H_2O molecules adsorb with energies of about 0.4 eV. In the vicinity of the peripheral interfacial sites of the Au cluster the calculations show that the adsorption energy of H_2O increases by 0.1 to 0.2 eV (depending on the particular site and adsorption configuration); thus, the gold cluster acts as an attractor for adsorbed water (reverse spillover). Hence, at the interface between the Au cluster and the MgO surface, peripheral sites show a high propensity to bind both H_2O and O_2 (Table 2). The markedly larger binding energies of the coadsorbed complex (compared to the individual adsorbates) reflect a synergetic effect, expressed through the occurrence of the aforementioned proton-sharing and proton-transfer processes.

To address the reactivity of O_2 coadsorbed with H_2O on the top facet of the adsorbed gold cluster, a sequence of adsorption and reaction steps that result in the catalytic oxidation of CO is displayed in Figure 8. Starting from the bare Au_8/MgO system, an H_2O molecule adsorbs first (Figure 8a). Subsequently, an O_2 molecule is coadsorbed and the system is exposed to incident CO (see the proton-sharing configuration in Figure 8b). In Figure 8c, a proton-transfer process induced by the incoming gaseous CO molecule is shown, which leads to the formation of a hydroperoxyl-like complex. Upon reaction

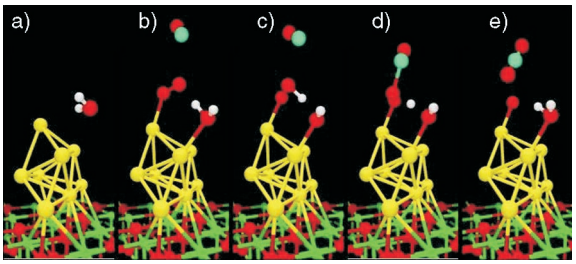

Figure 8. Relaxed atomic configurations, displaying several stages in the simulation of the coadsorption of H_2O and O_2 on the top-facet of an Au_8 cluster supported on MgO(100), and the subsequent reaction with gaseous CO to form CO_2. a) The approach of an H_2O molecule to the cluster. b) Coadsorbed H_2O (right) and O_2 (left) with an approaching CO. Note, the preferential orientation of the H_2O and partial proton-sharing. c) CO-induced proton transfer, resulting in formation of a hydroperoxyl-like group (left) and a hydroxyl (right). d) Transition state configuration with the CO binding to the activated species. The proton is about midway between one of the oxygens of the transition-state complex (left) and the hydroxyl (right). e) The proton shuttles back to reform an adsorbed H_2O, and the CO_2 product desorbs from the surface, leaving an adsorbed oxygen atom that reacts in the next step with a CO molecule, to yield a second CO_2. Spheres; Au (yellow), O (red), H (white) and C (magenta).

of the CO molecule with the complex, the proton shuttles back toward the hydroxyl group (Figure 8d), with the process culminating in the desorption of a CO_2 molecule and re-formation of an adsorbed H_2O molecule that is preferentially oriented with respect to the remaining adsorbed oxygen atom (Figure 8e). The above ER-like reaction mechanism involves relatively low barriers and the formation of the transition state (Figure 8d) entails a readily accessible energy barrier of $\approx$0.5 eV. An added CO molecule reacts readily (a barrier of 0.1 eV) with the single adsorbed oxygen atom, and the (barrierless) desorption of the CO_2 product closes the catalytic cycle. For a peripherally adsorbed O_2 molecule reacting with a CO molecule adsorbed in its vicinity, a Langmuir–Hinshelwood reaction barrier of 0.4 eV is found (with or without a neighboring coadsorbed H_2O molecule). The barrier for desorption of the CO_2 product is 0.6 eV under dry conditions and 0.3 eV with coadsorbed H_2O.

Summary

The current knowledge of the factors controlling the reactivity of small supported gold clusters at the molecular level has been discussed. It is shown that defect sites in the magnesium oxide support stabilize gold clusters. Whereas Au_8/MgO(defect-poor) is found to be inert, Au_8/MgO(FC) is highly active for CO oxidation. The key for understanding this change in reactivity is cluster charging. Calculations show that the F center in MgO leads to cluster charging, thus activating oxygen and carbon monoxide molecules adsorbed on Au_8. Experimentally, the cluster charging can be observed by a shift in the C–O stretch of adsorbed CO. By comparison, no cluster charging is found for Au_4/MgO(FC) and inactive catalysts. Another important factor controlling the reactivity of the gold cluster is structural fluxionality. Calculations show that the ability to dynamically adapt its structure, such as allowing the reaction to evolve on the most favorable free-energy path, is essential for its catalytic activity, since constraining the cluster to maintain its original geometry prevents the adsorption and activation of O_2. The promotional effect of water can be explained by the formation of an H_2O–O_2 complex, which involves partial proton sharing. Furthermore, the O–O bond is activated, thus facilitating the reaction with CO.

Acknowledgments

The presented research is supported by the German Research Council (DFG), the European Community through the GSOMEN project (Technical University Munich), the US Air Force Office of Scientific Research (AFOSR), and the Department of Energy (DOE), Georgia Institute of Technology.

Keywords: ab initio calculations · adsorption · gold · heterogeneous catalysis · supported catalysts

[1] B. Hammer, J. K. Norskov, *Nature* **1995**, *376*, 238.
[2] M. Haruta, *Cattech* **2002**, *6*, 102.
[3] D. Y. Cha, G. Parravan, *J. Catal.* **1970**, *18*, 200.
[4] G. C. Bond, P. A. Sermon, G. Webb, D. A. Buchanan, P. B. Wells, *J. Chem. Soc. Chem. Commun.* **1973**, 444.
[5] M. Haruta, N. Yamada, T. Kobayashi, S. Iijima, *J. Catal.* **1989**, *115*, 301.
[6] M. Haruta, *Gold Bull.* **2004**, *37*, 27.
[7] B. Nkosi, M. D. Adams, N. J. Coville, G. J. Hutchings, *J. Catal.* **1991**, *128*, 378.
[8] B. Nkosi, N. J. Coville, G. J. Hutchings, M. D. Adams, J. Friedl, F. E. Wagner, *J. Catal.* **1991**, *128*, 366.
[9] C. T. Campbell, *Science* **2004**, *306*, 234.
[10] M. S. Chen, D. W. Goodman, *Science* **2004**, *306*, 252.
[11] G. C. Bond, D. T. Thompson, *Gold Bull.* **2000**, *33*, 41.
[12] V. A. Bondzie, S. C. Parker, C. T. Campbell, *Catal. Lett.* **1999**, *63*, 143.
[13] V. A. Bondzie, S. C. Parker, C. T. Campbell, *J. Vac. Sci. Technol. A* **1999**, *17*, 1717.
[14] A. Sanchez, S. Abbet, U. Heiz, W. D. Schneider, H. Hakkinen, R. N. Barnett, U. Landman, *J. Phys. Chem. A* **1999**, *103*, 9573.
[15] B. Yoon, H. Hakkinen, U. Landman, A. S. Worz, J. M. Antonietti, S. Abbet, K. Judai, U. Heiz, *Science* **2005**, *307*, 403.
[16] L. M. Molina, B. Hammer, *Appl. Catal. A* **2005**, *291*, 21.
[17] O. Meerson, G. Sitja, C. R. Henry, *Eur. Phys. J. D* **2005**, *34*, 119.
[18] M. Haruta, S. Tsubota, T. Kobayashi, H. Kageyama, M. J. Genet, B. Delmon, *J. Catal.* **1993**, *144*, 175.
[19] M. Date, M. Haruta, *J. Catal.* **2001**, *201*, 221.
[20] M. Date, M. Okumura, S. Tsubota, M. Haruta, *Angew. Chem.* **2004**, *116*, 2181; *Angew. Chem. Int. Ed.* **2004**, *43*, 2129.
[21] T. V. Choudhary, D. W. Goodman, *Appl. Catal. A* **2005**, *291*, 32.
[22] B. Yoon, H. Hakkinen, U. Landman, *J. Phys. Chem. A* **2003**, *107*, 4066.
[23] N. Lopez, J. K. Norskov, *J. Am. Chem. Soc.* **2002**, *124*, 11 262.
[24] G. Mills, M. S. Gordon, H. Metiu, *Chem. Phys. Lett.* **2002**, *359*, 493.
[25] L. M. Molina, B. Hammer, *Phys. Rev. Lett.* **2003**, *90*, 206102.
[26] L. M. Molina, B. Hammer, *Phys. Rev. B* **2004**, 69.
[27] R. Meyer, C. Lemire, S. Shaikhutdinov, H. J. Freund, *Gold Bull.* **2004**, *37*, 72.
[28] C. Lemire, R. Meyer, S. Shaikhutdinov, H. J. Freund, *Angew. Chem.* **2004**, *116*, 121; *Angew. Chem. Int. Ed.* **2004**, *43*, 118.
[29] C. Lemire, R. Meyer, S. K. Shaikhutdinov, H. J. Freund, *Surf. Sci.* **2004**, *552*, 27.
[30] W. A. deHeer, *Rev. Mod. Phys.* **1993**, *65*, 611.
[31] T. G. Dietz, M. A. Duncan, D. E. Powers, R. E. Smalley, *J. Chem. Phys.* **1981**, *74*, 6511.
[32] U. Heiz, F. Vanolli, L. Trento, W. D. Schneider, *Rev. Sci. Instrum.* **1997**, *68*, 1986.
[33] U. Heiz, W. D. Schneider, *Crit. Rev. Solid State Mater. Sci.* **2001**, *26*, 251.

[34] M. Moseler, H. Hakkinen, U. Landman, *Phys. Rev. Lett.* **2002**, *89*, 033401.
[35] K. Bromann, H. Brune, C. Felix, W. Harbich, R. Monot, J. Buttet, K. Kern, *Surf. Sci.* **1997**, *377*, 1051.
[36] X. Tong, L. Benz, P. Kemper, H. Metiu, M. T. Bowers, S. K. Buratto, *J. Am. Chem. Soc.* **2005**, *127*, 13 516.
[37] S. Fedrigo, W. Harbich, J. Buttet, *Phys. Rev. B* **1998**, *58*, 7428.
[38] K. Judai, S. Abbet, A. S. Worz, U. Heiz, C. R. Henry, *J. Am. Chem. Soc.* **2004**, *126*, 2732.
[39] J. M. Antonietti, M. Michalski, U. Heiz, H. Jones, K. H. Lim, N. Rosch, A. Del Vitto, G. Pacchioni, *Phys. Rev. Lett.* **2005**, *94*, 213402.
[40] C. Di Valentin, A. Del Vitto, G. Pacchioni, S. Abbet, A. S. Worz, K. Judai, U. Heiz, *J. Phys. Chem. B* **2002**, *106*, 11 961.
[41] S. Lee, C. Y. Fan, T. P. Wu, S. L. Anderson, *J. Phys. Chem. B* **2005**, *109*, 11 340.
[42] S. S. Lee, C. Y. Fan, T. P. Wu, S. L. Anderson, *J. Am. Chem. Soc.* **2004**, *126*, 5682.
[43] M. Sterrer, E. Fischbach, T. Risse, H. J. Freund, *Phys. Rev. Lett.* **2005**, *94*, 186101.
[44] S. Schintke, W. D. Schneider, *J. Phys. Condens. Matter* **2004**, *16*, R49.
[45] M. Sterrer, M. Heyde, M. Novicki, N. Nilius, T. Risse, H. P. Rust, G. Pacchioni, H. J. Freund, *J. Phys. Chem. B* **2006**, *110*, 46.
[46] D. Peterka, C. Tegenkamp, K. M. Schroder, W. Ernst, H. Pfnur, *Surf. Sci.* **1999**, *431*, 146.
[47] G. Blyholder, *J. Phys. Chem.* **1964**, *68*, 2772.
[48] H. Hakkinen, W. Abbet, A. Sanchez, U. Heiz, U. Landman, *Angew. Chem.* **2003**, *115*, 1335; *Angew. Chem. Int. Ed.* **2003**, *42*, 1297.
[49] A. Bongiorno, U. Landman, *Phys. Rev. Lett.* **2005**, *95*, 106012.
[50] J. P. Perdew, K. Burke, M. Ernzerhof, *Phys. Rev. Lett.* **1996**, *77*, 3865.
[51] D. Vanderbilt, *Phys. Rev. B* **1990**, *41*, 7892.
[52] N. Troullier, J. L. Martins, *Phys. Rev. B* **1991**, *43*, 1993.

Received: January 12, 2006
Revised: March 21, 2006
Published online on August 1, 2006

